PHASE TRANSFORMATION AND FORCE-DEFLECTION RESPONSES OF NiTi ARCHWIRE FOR BRACKET ASSEMBLY IN ORTHODONTIC TREATMENT

MUHAMMAD FAUZINIZAM BIN RAZALI

UNIVERSITI SAINS MALAYSIA
2018

PHASE TRANSFORMATION AND FORCE-DEFLECTION RESPONSES OF NiTi ARCHWIRE FOR BRACKET ASSEMBLY IN ORTHODONTIC TREATMENT

by

MUHAMMAD FAUZINIZAM BIN RAZALI

Thesis submitted in fulfilment of the requirements
for the degree of
Doctor of Philosophy

January 2018

ACKNOWLEDGEMENTS

First of all, I am grateful to The Almighty God for giving me the opportunity to embark on my PhD and for completing this challenging journey successfully.

I wish to express my sincere thanks to Assoc. Prof. Ir. Dr. Abdus Samad for serving as a successful supervisor of this research project and for providing me with the insights and guidance. His understanding, valuable suggestion, wide knowledge and writing guidance have provided a good basis for the present thesis. Thanks also to my co-supervisor, Dr Norehan Mokhtar for her understanding, assistance, and knowledge regarding this research.

I would like to thank Universiti Sains Malaysia for the scholarship and research grant I have received. Sincere thanks to all academic and technical staff at the School of Mechanical Engineering, USM for their invaluable assistance in the mechanical background since my Bachelor's and Master's degree studies.

Last but not least, I would like to express deepest gratitude to my beloved mom (Khalijah) and dad (Razali), my lovely wife (Rohana), son (Firas) and daughters (Ayra and Aira) for their continuous love, support and encouragement. For those who have directly and indirectly contributed to the accomplishment of this thesis, thank you so much.

Muhammad Fauzinizam bin Razali

January 2018

TABLES OF CONTENTS

ACKNOWLEDGEMENT **ii**

TABLE OF CONTENTS **iii**

LIST OF TABLES **viii**

LIST OF FIGURES **ix**

LIST OF ABBREVIATIONS **xvi**

LIST OF SYMBOLS **xvii**

ABSTRAK **xviii**

ABSTRACT **xx**

CHAPTER ONE: INTRODUCTION 1

1.1 Research background 1

1.1.1 Fixed appliance therapy 1

1.1.2 Force-deflection of NiTi alloy during bending 5

1.1.3 Biomedical application of NiTi material: levelling treatment 6

1.2 Problem statement 10

1.3 Research objectives 11

1.4 Contribution of study 12

1.5 Scope of study 12

1.6 Thesis outline 13

CHAPTER TWO: LITERATURE REVIEW 14

2.1 Introduction 14

2.2 Unique mechanics of NiTi: thermal and mechanical behavior 14

2.3 Ideal force for tooth movement 20

2.4 Fixed appliance therapy 23

2.5 Leveling stage in orthodontic treatment 27

2.6 Classification of friction during sliding 28

2.7 Variables influencing friction in orthodontic 34

2.7.1 Archwire size 34

2.7.2 Surface roughness 36

2.7.3 Manufacturing process 38

2.7.4 Oral atmosphere 40

2.8 Force-deflection behavior during leveling 41

2.8.1 Bending model 41

2.8.2 Wire deflection 45

2.8.3 Ligation technique 48

2.8.4 Inter-bracket distance 49

2.8.5 Bracket composition 50

2.8.6 Oral atmosphere 51

2.9 Numerical method and finite element analysis 52

2.9.1 Shape memory alloy constitutive theory 52

2.9.2 Superelasticity during bending 56

2.10 Summary 61

CHAPTER THREE: EXPERIMENTAL DESIGN AND PROCEDURE 65

3.1 Introduction 65

3.2 Experimental testing 65

3.2.1 Calorimetric analysis 65

3.2.2 Tensile test 66

3.2.3 Three-bracket bending test 67

3.2.4 Three-point bending test 70

3.2.5 Dimensional and composition determination 71

3.2.6 Surface roughness measurement 71

3.2.7 Sliding test 72

3.3 Development of three-bracket bending model 74

3.3.1 Verification of material parameters 74

3.3.2 Generation of part, mesh and assembly of the model 78

3.3.3 Discretization of contact surfaces 81

3.3.4 Boundary conditions and analysis step 84

3.3.5 Mechanical convergence study 86

3.4 Development of three point bending model 89

3.5 Design of experiment 90

CHAPTER FOUR: RESULTS AND DISCUSSION 94

4.1 Introduction 94

4.2 Archwire and bracket properties 94

4.2.1 Archwire composition 94

4.2.2 Surface roughness of archwire and bracket 95

4.2.3 Thermal and mechanical properties of NiTi archwire 96

4.2.4 Frictional properties 100

4.3 Validation of finite element model 101

4.3.1 Uniaxial deformation 101

4.3.2 Force deflection in a three-bracket bending setup 103

4.3.3 Force deflection in three-point bending 107

4.3.4 Evolution of phase transformation during bending 109

4.3.5 Evolution of binding friction during bending 113

4.4 Variation in the NiTi archwire's phase transformation and bending deformation during levelling 120

4.4.1 Propagation of principal stress 120

4.4.2 Propagation of martensite fraction 125

4.4.3 Extent of wire deformation at different bending settings 127

4.5 Development of regression model for archwire force prediction 130

4.5.1 Design of experiment (DOE) 130

4.5.2 Regression model and analysis of variance (ANOVA) 134

4.5.3 Central composite design results 136

4.6 NiTi archwire's force-deflection behaviour at different bending settings 137

4.6.1 Maximum force transmitted during wire activation 137

4.6.2 Minimum force transmitted during deflection recovery 141

4.6.3 Slope of the deactivation curve 144

4.7 Force-deflection behaviour of NiTi archwire with different bracket coupling 148

4.7.1 Force-deflection curve 148

4.7.2 Variation of binding during bending 153

4.7.3 Variation of archwire forces during bending 154

CHAPTER FIVE: CONCLUSIONS AND FUTURE WORKS 161

5.1 Evolution of phase transformation 161

5.2 Correlation between binding and force-deflection behaviour 162

5.2.1 Effect of bending setting 162

5.2.2 Effect of friction coefficient 163

5.3 Recommendations for future works 164

REFERENCES 165

APPENDICES

Appendix A: Sample calculation of wire deflection

LIST OF PUBLICATIONS

LIST OF TABLES

		Page
Table 1.1	Available sizes for round and rectangular archwires	5
Table 2.1	Types of tooth movements	21
Table 2.2	Summary of material parameters requires by UMAT of Auricchio and Taylor formulation	55
Table 2.3	Summary of testing settings used for levelling treatment in-vitro studies	62
Table 3.1	Combination of bending setting for the validation with the numerical result	70
Table 3.2	The mechanical properties and the shape memory deformation behaviours of the NiTi archwires used in this study, measured form the uniaxial stress-strain curve	76
Table 3.3	Displacement-based analysis set, used to verify the reliability of the selected material parameters	77
Table 3.4	Total number of element used for each model part	79
Table 3.5	Summary of boundary conditions applied on each reference point	86
Table 3.6	Summary of the mesh refinement model	88
Table 3.7	Testing ranges considered for each setting	91
Table 4.1	Average atomic composition of NiTi archwire	95
Table 4.2	Average surface roughness of NiTi wires and dental brackets	95
Table 4.3	Actual and coded values for each central composite design factor	131
Table 4.4	Summary of the force data obtained from the force-deflection curves	133
Table 4.5	Summary of ANOVA for the maximum force (Y_1), the minimum force (Y_2), and the force slope (Y_3)	135
Table 4.6	Maximum force of NiTi archwire at different bending settings	139
Table 4.7	Minimum force of NiTi archwire at different bending settings	142
Table 4.8	Force slope of NiTi archwire during deactivation at different bending settings	145

LIST OF FIGURES

		Page
Figure 1.1	Ligation of a markedly irregular canine tooth	1
Figure 1.2	Comparison of ligating mechanisms and slot dimensions between an active and a passive self-ligating bracket	2
Figure 1.3	Comparison of visual appearances between a conventional (stainless steel) and an aesthetic bracket (ceramic)	3
Figure 1.4	Common curvatures of orthodontic archwires: (a) natural arch shape and (b) standard shape	4
Figure 1.5	Simple bending of orthodontic archwires: (a) three-point bending model and (b) force-deflection comparison between NiTi, stainless steel, and beta titanium archwires	6
Figure 1.6	Schematic representation of sliding resistance components in a fixed appliance system	8
Figure 1.7	Modified bending of orthodontic archwire: (a) three bracket bending model and (b) force-deflection of NiTi wire	9
Figure 1.8	Schematic representation of the existing archwire drawing model: (a) wire slides over a tilted bracket and (b) over a displaced bracket	10
Figure 2.1	Typical DSC curve of shape memory alloy	17
Figure 2.2	Stress-strain-temperature curve of shape memory effect behaviour	18
Figure 2.3	Stress-strain curve of superelasticity	19
Figure 2.4	Superelastic stress-strain curves of NiTi alloy at various testing temperatures	20
Figure 2.5	Application of NiTi closing coils in the right quadrant	22
Figure 2.6	Scanning electron micrographs of the self-ligating brackets	24
Figure 2.7	The upper incisor and canine angulations required by various prescriptions	25

		Page
Figure 2.8	Scanning electron micrographs of (a) elastomer and (b) wire ties used to secure the archwire inside the bracket slot	26
Figure 2.9	Trigonometric representation of archwire deflection, with respect to vertical bracket displacement	28
Figure 2.10	Determination of static and kinetic friction from the force plot	29
Figure 2.11	Bracket positioning jig for the straight-wire-drawing method	30
Figure 2.12	Drawing test model used to measure sliding resistance at the archwire-bracket interface (by allowing bracket tipping)	31
Figure 2.13	Drawing test model used to find the static friction: a) an archform plate and b) the end of an archwire held by the gripper	32
Figure 2.14	The schematic representation of the critical angle for binding, with respect to the tipping angle of the bracket	32
Figure 2.15	Schematic diagram showing the partition of the resistance to sliding (RS) into its' components, namely, ligating friction (FL), elastic binding (BI), and physical notching (NO)	33
Figure 2.16	Simulated high maxillary right canine, using an orthodontic simulator	36
Figure 2.17	Scanning electron micrographs of ceramic bracket slots; (a) with metal layer and (b) without the metal layer	38
Figure 2.18	Scanning electron microscope photomicrographs of inner-slot bracket surfaces: (a) as-received specimen; (b) DLC-coated specimen	39
Figure 2.19	Deactivation curves for superelastic NiTi archwires of different sizes	42
Figure 2.20	A schematic of a centrally loaded wire undergoing a three-point bending test	43
Figure 2.21	Force-deflection comparison between superelastic NiTi and several other orthodontic materials	44
Figure 2.22	Force-deflection curves using (a) three-point bending and (b) arch bracket bending	45

		Page
Figure 2.23	Three-bracket bending setting, used to simulate a high maxillary right canine	45
Figure 2.24	NiTi archwire force-deflection curves at several deflection magnitudes	46
Figure 2.25	Deactivation curve registered by a 0.36-mm NiTi archwire at different deflection magnitudes	47
Figure 2.26	NiTi wire force-deflection curves at different deflection magnitudes, obtained from three-point bending tests	48
Figure 2.27	Average midpoint distances between maxillary teeth	50
Figure 2.28	Force-deflection curves of 0.46 × 0.64-mm archwire at 25°C, 37°C, and 50°C	52
Figure 2.29	Comparison of stress-strain curve of superelastic NiTi wire obtained from the experimental, Auricchio and Lagoudas model calculation	53
Figure 2.30	Mechanical properties required by UMAT/Nitinol: a) stress-strain curve and b) stress-temperature curve	56
Figure 2.31	Normal strain distribution over a beam under a bending load	57
Figure 2.32	Distribution of bending stress across the wire section undergoing bending-type deformation	58
Figure 2.33	Strain field of a tube undergoing four-point bending	59
Figure 2.34	NiTi archwire bending behaviour in a bracket system: (a) stress-strain curve of most tensioned element and (b) the stress contour plot at the 3.0-mm deflection	60
Figure 3.1	Tensile test setup, equipped with a heating chamber	67
Figure 3.2	NiTi wire, bent on three-bracket bending setup	68
Figure 3.3	NiTi specimen bent on three points bending setup	71
Figure 3.4	Sliding test setup on: (a) a pin-on-disk tribometer equipment and (b) schematic diagram of the positioning of archwire and bracket	73
Figure 3.5	Three-bracket bending model development flow chart	74

		Page
Figure 3.6	Illustration of selected points on the NiTi archwire specimen stress-strain curve	75
Figure 3.7	One-element model, used to verify the superelastic behaviour during uniaxial deformation	77
Figure 3.8	Illustration of a reduced-integration hexahedral element	78
Figure 3.9	Bending behaviour for a single first-order reduced-integration element	79
Figure 3.10	Illustration of mesh densities: (a) round wire, (b) rectangular wire, (c) bracket, and (d) scanning electron micrographs of stainless steel bracket geometry	80
Figure 3.11	Positioning of archwire and brackets during the assembly stage	81
Figure 3.12	Selection of master and slave surfaces for contact pairing at the middle bracket	82
Figure 3.13	Default pressure-overclosure relationship	83
Figure 3.14	Coulomb model for the tangential interaction	84
Figure 3.15	Boundary and load conditions applied on the three-bracket model	85
Figure 3.16	Element meshes of 0.40 mm wire at different global element size of (a) 0.07 mm, (b) 0.04 mm and (c) 0.03 mm	87
Figure 3.17	Variation of stabilization and internal energies of the three-bracket bending model upon the use of 0.4 mm archwire	88
Figure 3.18	Boundary and load conditions applied on the three-bracket mode	89
Figure 3.19	Summary of pre-processing input and post-processing output, investigated in the present study	91
Figure 4.1	SEM images of the bracket surface at 250 times magnification: a) stainless steel bracket and b) ceramic bracket	96
Figure 4.2	Thermal transformation behaviours of NiTi archwires: (a) round wire and (b) rectangular wire	97

		Page
Figure 4.3	Stress-strain curves of NiTi archwires undergoing the uniaxial test at 26°C	98
Figure 4.4	Variations in the critical stresses of forward and reverse stress-induced martensitic transformations	99
Figure 4.5	Stress-strain curves of NiTi archwires prior to uniaxial tension at 36°C	100
Figure 4.6	Plot of frictional forces and friction coefficients along the sliding distance	101
Figure 4.7	Stress strain curve of NiTi wire under numerical and experimental uniaxial test at different temperatures: (a) 26°C, (b) 36°C and (c) 46°C	102
Figure 4.8	Stress-strain curve produced by the one-element model during uniaxial deformation at 26°C	103
Figure 4.9	Post-processing output, with the middle bracket as the reference point: (a) vertical reaction force (RF2) and (b) vertical bracket displacement (U2)	104
Figure 4.10	Direction and size of the middle bracket reaction force arrow during the (a) activation and (b) deactivation of NiTi archwire at 3.5 mm deflection	105
Figure 4.11	Force-deflection comparisons between the numerical and the experimental bending of the NiTi archwire at different bending settings	106
Figure 4.12	Force-deflection curve of the NiTi arch wire, bent in the three-point bending setup at 26°C	108
Figure 4.13	Force-deflection curves of NiTi archwire obtained from the three-point and the three-bracket bending tests	109
Figure 4.14	Force-deflection curve of the NiTi archwire, bent under frictionless setting in the three-point bending model	110
Figure 4.15	View cut of NiTi archwire principal stress distribution upon activation at 3.1 mm and at 26°C	112

		Page
Figure 4.16	Illustration of strain and stress profile along the cross section of NiTi wire at: (a) 1.5-mm deflection, (b) 3.1-mm deflection and (c) stress-strain curve at the time of loading	113
Figure 4.17	Estimation of wire length addition at the 3.1-mm deflection	114
Figure 4.18	Force-deflection curve of the superelastic NiTi wire undergoing bending at 26°C in: (a) three-point bending model and (b) three-bracket bending model	116
Figure 4.19	Variation in binding generated during NiTi archwire bending, using: (a) three-point bending model and (b) three-bracket bending model	118
Figure 4.20	View cut of principal stress variation along the wire curvature at the middle bracket	119
Figure 4.21	Force-deflection behaviour of the NiTi archwire at different deflection magnitudes (numerical results)	120
Figure 4.22	Evolution of maximum archwire principal stress at different deflection magnitudes	121
Figure 4.23	Illustration of the location of the four elements near the critically bent region	122
Figure 4.24	Stress-strain plots of several elements, at different locations on the wire curvature	122
Figure 4.25	Finite element analysis of: (a) strain distribution, (b) stress distribution, and (c) the path defined across the thickness of the cross section	124
Figure 4.26	Stress-strain curves of a highly tensioned element at 1.0-mm, 2.0-mm, 3.0-mm, and 4.0-mm middle bracket displacements	125
Figure 4.27	Evolution of the archwire's martensite volume at different deflection magnitudes	126
Figure 4.28	Variation in the NiTi archwire’s maximum principal stress during activation, at different bending temperatures	128
Figure 4.29	Variation in the NiTi archwire's maximum principal stress during activation at different inter-bracket distance settings	129
Figure 4.30	Force-deflection behaviour of the NiTi archwire bent at different deflection magnitudes	132

		Page
Figure 4.31	Graphs of predicted versus actual values for: (a) maximum force, (b) minimum force, and (c) force slope	137
Figure 4.32	The maximum-force perturbation plot (Note: *A* = inter-bracket distance, *B* = wire deflection, and *C* = testing temperature)	141
Figure 4.33	The minimum-force perturbation plots (Note: *A* = inter-bracket distance, *B* = wire deflection, and *C* = testing temperature)	144
Figure 4.34	Force slope perturbation plots (Note: *A* = inter-bracket distance, *B* = wire deflection, and *C* = testing temperature)	147
Figure 4.35	Force-deflection curves for (a) 0.4 mm × 0.56 mm rectangular wire, (b) 0.4 mm round wire, and (c) 0.3 mm round wire, with varied friction coefficients	150
Figure 4.36	Force-deflection curves of 0.4-mm NiTi wires prior to bend in the presence of stainless steel and ceramic bracket	152
Figure 4.37	Plot of frictional force obtained from sliding the NiTi archwire along the slot of the stainless steel and ceramic brackets	153
Figure 4.38	Maximum binding encountered by the NiTi archwire during: (a) activation and (b) deactivation cycle	154
Figure 4.39	Maximum force exerted by NiTi archwires at various friction coefficients	155
Figure 4.40	Minimum force exerted by NiTi archwires at various friction coefficients	157
Figure 4.41	Force slope of NiTi archwires at various friction coefficients	158

LIST OF ABBREVIATIONS

SMA	Shape memory alloys
SIMT	Stress-induced martensitic transformation
UMAT	User material
DSC	Differential scanning calorimeter
SEM	Scanning electron microscope
UTM	Universal testing machine
NiTi	Nickel titanium
EDS	Energy dispersive X-ray spectroscopy
XRD	X-ray diffraction
ISO	International organization for standardisation
IBD	Inter-bracket distance
ANOVA	Analysis of variance
BI	Binding

LISTS OF SYMBOLS

A_s	Austenite start temperature
A_f	Austenite finish temperature
M_s	Martensite start temperature
M_f	Martensite finish temperature
μ_s	Static coefficient of friction
σ_s^{AS}	Critical stress for start of forward transformation
E_A	Austenite elasticity
E_M	Martensite elasticity
I	Area moment of inertia

PENJELMAAN FASA DAN TINDAK BALAS DAYA-DEFLEKSI DAWAI ARKUS NiTi BAGI PEMASANGAN PENDAKAP DALAM RAWATAN ORTODONTIK

ABSTRAK

Dawai arkus NiTi digunakan secara meluas di peringkat awal rawatan ortodontik kerana ciri-ciri super-elastik dan biokompatibiliti. Walaupun dawai arkus super-elastik NiTi sering digunakan di setiap peringkat rawatan ortodontik, evolusi penjelmaan fasa dan tingkah laku daya-defleksi dawai ini ketika dilenturkan dalam sistem pendakap masih kurang diketahui. Oleh kerana perubahan lenturan sering ditemui semasa rawatan pengarasan gigi, tahap ubah bentuk dawai dan geseran akan mengubah tingkah laku daya-defleksi dan seterusnya menjauhi kriteria daya optimum.

Kajian ini menyiasat evolusi penjelmaan fasa dan daya yang dikeluarkan oleh dawai arkus NiTi semasa rawatan pengarasan. Model unsur terhingga tiga dimensi bagi lenturan dawai arkus NiTi dalam konfigurasi tiga pendakap gigi telah dibangunkan dengan menggunakan subrutin bahan dan interaksi sentuh. Pekali geseran yang diperlukan untuk menentukan hubungan antara dawai dan pendakap keluli tahan karat diperoleh daripada ujian geluncur. Kecekapan model ini diperiksa dengan membandingkan ramalan lengkung daya-defleksi dengan keputusan eksperimen. Penyelidikan ini meningkatkan pengetahuan terkini tentang pengaruh geseran kepada tingkah laku daya-defleksi dawai arkus NiTi melalui kajian kuantitatif pada dua keadaan; melentur dawai pada pelbagai konfigurasi pengarasan (jarak antara pendakap, lenturan dawai dan suhu mulut) dan melentur dengan padanan pendakap yang diperbuat dari bahan yang berbeza (nilai pekali geseran diubah antara 0.1 hingga 0.5).

Semasa melentur, hanya sebahagian kecil panjang dawai mengalami transformasi daripada austenit ke martensit manakala selebihnya tidak mengalami sebarang ubahbentuk. Dawai yang diaktifkan pada 2.0 mm menghasilkan tegasan maksimum pada plateau tegasan, menunjukkan bahawa ubah bentuk dawai NiTi disebabkan oleh transformasi martensit yang diaruh tegasan. Dawai yang dilenturkan sehingga 3.0 mm dan 4.0 mm menghasilkan tegasan maksimum pada garis elastik martensit. Penambahan magnitud geseran di pinggir pendakap gigi meningkatkan daya maksimum dan cerun lengkung penyahaktifan dengan ketara, disamping mengurangkan nilai daya minimum. Bagi kes lenturan 4.0-mm, dawai berdiameter 0.4-mm menghasilkan daya di antara 0.13 N sehingga 0.73 N, yang mana dalam julat daya optimum untuk mencapai gerakan gigi yang effektif. Nilai geseran tertinggi bermagnitud 8.33 N dan 3.72 N telah dihasilkan ketika melentur dawai 0.40 × 0.56-mm dan 0.4-mm sebanyak 4.0 mm pada suhu 46°C dengan menggunakan jarak antara pendakap 7.0 mm. Model regresi yang dibangunkan boleh digunakan untuk menjangka daya-defleksi dawai NiTi, khususnya bagi sistem pendakap yang dikaji. Pemadanan dawai bulat dengan pendakap seramik ($\mu \geq 0.4$) menghasilkan daya bermagnitud sifar di awal urutan penyahaktifan, seterusnya menghalang gerakan gigi yang diperlukan.

PHASE TRANSFORMATION AND FORCE-DEFLECTION RESPONSES OF NiTi ARCHWIRE FOR BRACKET ASSEMBLY IN ORTHODONTIC TREATMENT

ABSTRACT

NiTi archwires are used widely during the early stage of orthodontic treatment due to its superelastic and biocompatibility properties. Even though the superelastic NiTi archwires are always preferred in most orthodontic treatments, the evolution of phase transformation and force-deflection behaviour of this wire subjected to bend in the bracket system is still uncertain. Since changes in bending setting are frequently encountered during levelling, the extent of wire deformation and binding friction at the wire-bracket interface would alter the force-deflection behaviour and subsequently defies the optimal force criteria.

This study investigated the evolution of phase transformation and forces released by NiTi archwire during orthodontic levelling treatment. For this purpose, a three-dimensional finite-element model of superelastic NiTi wire bends in three-bracket configurations was developed by employing a user material subroutine of superelasticity and contact interaction. The friction coefficient required to define the contact between the wire and stainless steel bracket was obtained from a sliding test. The competency of the bending model was examined by comparing the predicted force-deflection curve with the experimental results. The work further advanced the current knowledge on the influence of binding towards the force-deflection behaviour of NiTi wire by performing a quantitative study at two levelling conditions; bending at different levelling settings (inter-bracket distance, wire deflection and oral

temperature) and bending with the presence of different bracket materials (friction coefficient at contact locations were varied from 0.1 to 0.5).

During bending, only a small section of the wire length underwent austenite to martensite transformation, leaving the rest of the length substantially undeformed. The wire activated to 2.0 mm produced the maximum stress on the stress plateau, implying that the NiTi wire was deformed by stress-induced martensitic transformation. The wire activated to 3.0 mm and 4.0 mm essentially produced the maximum stress on the elastic line of martensite. The generation of binding at the bracket edges significantly elevated the maximum force and the slope of the deactivation curve, whilst diminished the minimum force values. The greatest binding of 8.33 N and 3.72 N was generated by the 0.40 × 0.56-mm and 0.4-mm archwires at the maximum deflection (4.0 mm) and temperature readings (46°C), and at the minimum inter-bracket distance (7.0 mm). For the case of large tooth displacement (4.0 mm), the 0.4-mm archwire delivered force in between 0.13 N to 0.73 N, which are within the optimal force range. The developed regression model can be used to predict the force-deflection of NiTi wire for the studied bracket system. Additionally, the archwires coupled with the ceramic brackets ($\mu \geq 0.4$) produced zero force magnitude at the onset of the deactivation cycle, thus inhibited further tooth movement.

CHAPTER ONE

INTRODUCTION

1.1 Research background

1.1.1 Fixed appliance therapy

Patients mainly seek orthodontic treatment to improve dental appearance (Abdullah, 2001). Most orthodontic treatments are carried out using fixed appliance therapy, as it promotes accurate tooth positioning (Angel, 1928). Figure 1.1 shows the main components of the fixed appliance used in a famous malocclusion case of a highly displaced canine tooth. The installation of the appliance is started by bonding the dental brackets on the tooth, before an archwire is carefully placed inside the bracket slot by following the irregularity of the bracket position, hence inducing localized bending across the wire length. Then, the archwire is secured inside the slot with the help of small rubber rings, fine wires, or metal door, depending on the ligation type of the chosen bracket. As the archwire tries to regain its' straight shape throughout the treatment duration, the malposed tooth is slowly pulled downwards, in the bending recovery direction.

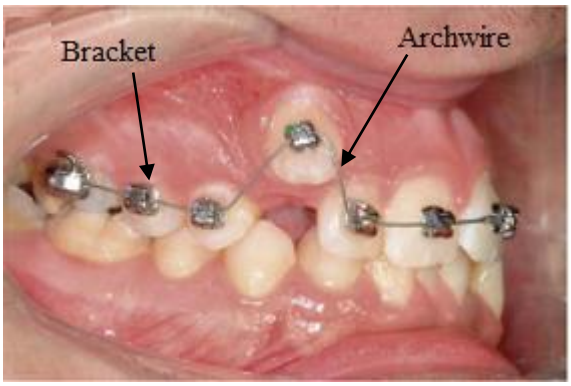

Figure 1.1 Ligation of a markedly irregular canine tooth (Graber et al., 2016)

On average, fixed braces usually last from 18 to 36 months (Hwang et al., 2001), and longer treatment will be required for teeth further out of position. A healthier tooth movement rate was reported to be around 1.0 mm per month, which can be achieved by applying a force of strength between 0.10 N and 1.20 N (Mitchell, 2013; Proffit et al., 2014). Forces within this range are efficient, in terms of providing maximum patient comfort (Krishnan and Davidovitch, 2006) and negligible permanent damage to the supporting periodontal tissues (Noda et al., 2010; Gonzales et al., 2008).

Commercial orthodontic brackets in the market can be categorized into conventional and self-ligating brackets. A conventional bracket uses elastomer ties or stainless steel ties to secure the archwire inside the bracket slot, whilst a self-ligating bracket uses its' built-in clip to keep the archwire within the slot. Additionally, self-ligating brackets are available in two types, active and passive. Figure 1.2 shows the mechanisms and the slot dimensions for both bracket types. The clip on the active bracket is designed to continuously press the archwire towards the slot base, hence promoting full control for finishing and detailing. In contrast, no pressing mechanism is designed for the passive bracket, and the deeper slot depth allow the archwire to slide freely along the slot.

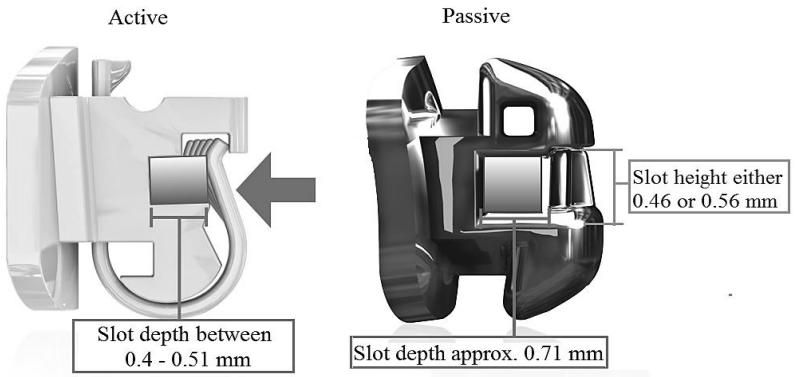

Figure 1.2 Comparison of ligating mechanisms and slot dimensions between an active and a passive self-ligating bracket (S. Samawi, 2014)